International Scholarly Research Network
ISRN Chemical Engineering
Volume 2012, Article ID 954869, 7 pages
doi:10.5402/2012/954869

Research Article

Effect of Sintering Temperatures on the Synthesis of SnO_2 Nanospheres

Bharat G. Pawar,[1] Dipak V. Pinjari,[2] Sanjay S. Kolekar,[1] Aniruddha B. Pandit,[2] and Sung H. Han[3]

[1] *Material Science and Electrochemistry Research Laboratory, Department of Chemistry, Shivaji University, Kolhapur 416004, India*
[2] *Chemical Engineering Division, Institute of Chemical Technology, Matunga, Mumbai 400019, India*
[3] *Inorganic Nano-Material Laboratory, Department of Chemistry, Hanyang University, Seoul 133-791, Republic of Korea*

Correspondence should be addressed to Sanjay S. Kolekar, kolekarss2003@yahoo.co.in

Received 17 February 2012; Accepted 6 March 2012

Academic Editors: R. M. Leblanc, L. Liotta, and I. Poulios

In this communication we report the rapid nanostructure of SnO_2 with a spherical morphology which has been prepared in large scale via sol-gel method. The products were characterized with scanning electron microscopy, X-ray powder diffraction, transmission electron microscopy, FTIR, and photoluminescence spectroscopy. The strong photoluminescence of the nanosphere in visible region suggested possible application in nanoscaled optoelectronic devices. A possible growth mechanism for the SnO_2 nanosphere in terms of solvation, hydrolysis, and polymerization was proposed.

1. Introduction

Nanometer-sized materials have recently attracted a considerable amount of attention due to their unique electrical, physical, chemical, and magnetic properties as well as their potential for technological applications [1]. Semiconductor nanoparticles have been extensively studied from both experimental and theoretical views—points owing to their potential application in solar energy conversion, photocatalysis, and optoelectronic industry [2]. Tin oxide (SnO_2), a n-type semiconductor with a wide band gap (3.6 eV, at 300 K), is well known for its potential applications in gas sensors, dye sensitized solar cells, and transparent conducting electrodes and as a catalyst support [3, 4]. Therefore, many processes have been proposed to synthesize SnO_2 nanostructures; some involve dry processes such as sputtering from tin oxide target [5] or from metallic target followed by oxidation [6] and chemical vapour deposition (CVD) [7], while others are based on wet processes, including spray pyrolysis [8] and sol-gel-related methods which have been used to prepare tin oxide coating, particles, and precipitates [9–15].

One of the most widely used, solution-based nanoparticle synthesis methods is the sol-gel process which involves the evolution of an inorganic network, known as sol, from certain precursor material and consequent gelation of this inorganic network to form ordered three-dimensional gel structure. The next step in the process is the destruction of the evolved gel, thus, resulting in the formation of nanocrystalline material [16]. The sol-gel process is widely used for manufacturing nanoparticles of different metal oxide materials like SnO_2 [17, 18], TiO_2 [19], ZnO [20, 21], and SiO_2 [22]. Amongst various methods, sol-gel process is a relatively novel process for the preparation of functional material that needs precise microstructural control in order to satisfy desired properties [23]. Sol-gel method has advantage of low cost and does not need complicated equipments and could be carried out at more or less ambient conditions, so this method is adopted and applied to synthesize tin oxide nanocrystalline powder.

In the presented work, nanocrystalline SnO_2 powder was synthesized using sol-gel route and possible sol-gel growth mechanism was proposed. The cost of the starting precursor used to synthesize nanomaterial decides the cost of the

final product. Tin chloride was used as precursor which is cheap as compared to the granulated tin and tin alkoxide. It offers the synthesis of nanocrystalline SnO_2-monodispersed particles of nanometer sizes with very large surface area. To the best of the author knowledge this is the first report on calculating percent crystallinity and crystalline size of the sol-gel-synthesized nanocrystalline SnO_2 powder, against sintering temperature.

2. Experimental

2.1. Preparation of Powder. The SnO_2 sol was prepared by dissolving 1.5 g tin chloride dihydrate (95% $SnCl_2 \cdot 2H_2O$, Merck, India) and 5 g citric acid (99.5% $C_6H_8O_7 \cdot H_2O$, Merck, India) in 8 M HNO_3 in a conical flask until a clear solution was obtained. Aqueous ammonia (25%, s d fine-chem Ltd., Mumbai, India) was added dropwise into the solution with stirring, until a pH of 9 was reached. The sol thus prepared was found to be transparent and stable with no precipitation or turbidity. The obtained sol was refluxed at 373 K for 2 h upon which it slowly turned into a turbid colloidal solution. After 5-6 h, the gel was separated via decantation, washed several times with double distilled water and ethanol to remove impurities. After drying at 373 K for 5 h in a hot air oven, the dried gel powder was ground in a mortar and finally sintered in muffle furnace at 373, 473, 573, 673, 773, 873, 973, 1073 K for 2 h.

2.2. Characterization of Powder. A detailed elucidation of the structure and composition was carried out by various characterization techniques. The structural elucidations of SnO_2 nanoparticle were carried out using X-ray diffractometer (XRD) (Rigaku MiniFlex at angle between 2 and 80° with scan rate of 2°/min, using Cu Kα_1 radiation = 1.5418 Å). The crystallite size was determined based on XRD peak broadening, was confirmed by transmission electron microscope (TEM) (Omega EM 912, operated at 200 kV), and was used for grain size confirmation. Sample for TEM investigation was prepared by putting an aliquote of dichloromethane solution of SnO_2 nanoparticles onto an amorphous carbon substrate supported on a copper grid. Surface area, pore volume, and pore diameter were obtained from BET (Micrometer ASAP 2010 Instrument, USA) examination. The surface morphology and size of SnO_2 particle were analyzed by using the scanning electron microscope (SEM) (JOEL JSM 680 LA15 KV). The elemental stoichiometry for the quantitative elemental analysis was obtained from the energy dispersive X-ray analyzer.

3. Result and Discussion

The XRD patterns of all the samples of SnO_2 nanoparticles at different sintering temperatures from 373 K–1073 K are shown in Figure 1. The samples, namely, a, b, c, d, e, f, g, and h, are referred with respect to their sintering temperatures of 373–1073 K, respectively. The formation of tetragonal rutile structural phase is confirmed and the peaks obtained are well matched with the JCPDS card no. 14-1445.

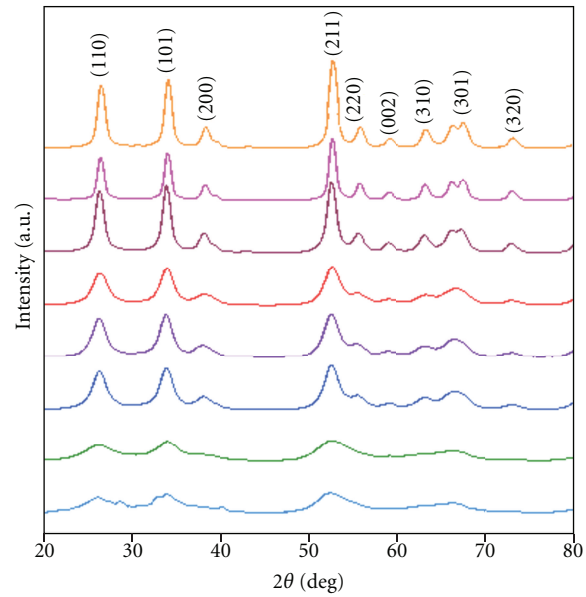

Figure 1: XRD pattern of the nanosized SnO_2 nanoparticles synthesized by sol-gel method, sintering at temperature step at 373–1073 K.

The XRD plot of the powder samples sintered at different temperature shows increase in the peak intensity values with respect to temperature of sintering thereby showing an increasing crystallinity of the samples with an increasing sintering temperature. Further, it is observed that at lower temperature the peaks are not well resolved indicating the presence of amorphous phase, and secondly the sintering temperature increased indicating the removal of impurities and the formation of crystalline phase. The peak orientations in the planes (110), (101), (200), (211), (220), (002), (310), (112), (301), and (321) clearly indicate the effective growth of the nanostructure in the X-direction. The peak with orientation (301) starts to split at the temperature of 873 K, indicating that higher crystallinity of the material is obtained at high temperature. The width of reflection is considerably broadened, indicating a small crystalline domain size. The broadening decreases with an increase of heat treatment temperature in the range of 373−1073 K.

Crystalline size "D" was obtained by the measurement of the broadening of diffraction lines and applying the Debye-Scherrer formula [24]:

$$D = \frac{0.94\lambda}{\beta \cos\theta}, \tag{1}$$

where λ is the wavelength of Cu Kα_1 radiations (1.5418 Å), β the full-width at half-maximum of the peaks corresponding to the plane, and θ the angle obtained from 2θ value corresponding to a maximum intensity peak in XRD pattern. The crystalline size of obtained SnO_2 particles was varying from 3 to 17 nm, as shown in Figure 2.

The % of crystallinity of specimen is an indication of the uniformality of lattice structure in the specimen. A sample with higher crystallinity would show improved properties

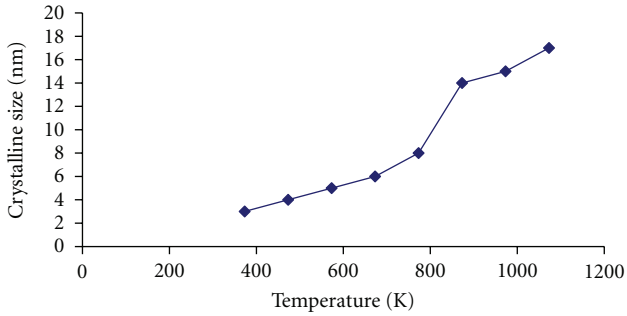

Figure 2: Variation of the crystalline size of the SnO_2 nanoparticles with sintering temperature step, 373–1073 K.

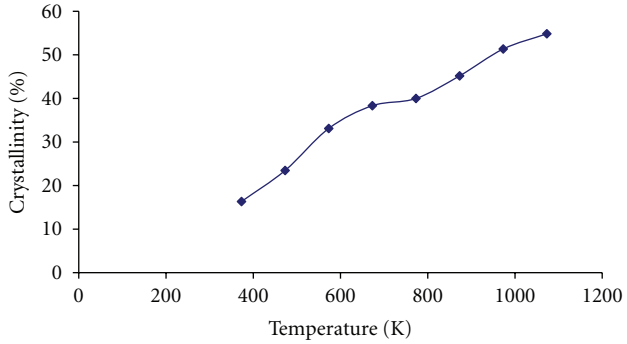

Figure 3: Variation of the crystallinity of the SnO_2 nanoparticles with sintering temperature step, 373–1073 K.

such as packing density and stability, than one with relatively lower crystallinity. The amorphous content of the sample may be determined by taking the ratio of the amorphous area of the X-ray diffractogram to the total area. By amorphous area we mean that area of diffractogram is not contained by any specific diffraction peak. In the past, we have successfully used this method for determining the % crystallinity of metal oxide [25, 26]. The process involves the following:

(i) smoothing the diffraction graph by a suitable smoothening method (Savitzky-Golay method is preferred);

(ii) creating a baseline for the diffractogram whereby all the peaks shall be essentially starting at a common base. This is done by making use of the Sonnefield-Visser method obtained as part of the software;

(iii) computing integral area which is nothing but the crystalline area of the material;

(iv) now the total area of the diffractogram is computed by carrying out this entire operation except that baseline is not created;

(v) now 100 times the ratio of crystalline area to the total area is the % crystallinity;

(vi) 100 minus the % crystallinity is indicated as the amorphous content;

The phase transformation is a temperature-dependant process. We observed that as sintering temperature increases, % of crystallinity increases and it ranges in between 16–54%. The sample sintering at 1073 K shows highest crystallinity, that is, 54.84%, while sample sintered at 373 K shows lowest crystallinity percentage, that is, 16.33%. Figure 3 shows the % increase in crystallinity with an increase in the sintering temperature.

Figure 4(a) exhibits an intense, very broad IR peak ranging from 3600–2500 cm^{-1} with maxima at 3126 cm^{-1} which may be due to absorbed water and ammonia. As heat treatment increases above 873 K, peak at 3126 cm^{-1}, due to ammonia completely disappears after calcination (Figure 4(b)). The peak at 1383 cm^{-1} can be ascribed to the bending vibration of NO_3^- ions occluded into the gel [2, 27]. The peaks are reduced as the calcination temperatures are increased. The next peak obtained between (1232–900 cm^{-1}) is attributed to the hydroxyl-tin vibrations [28]. The peak at 625 cm^{-1} and 519 cm^{-1} are attributed to Sn-O stretching modes of Sn-Sn-O and Sn-OH, respectively.

The scanning electron microscopy images of the SnO_2 nanoparticle prepared by sol-gel method and the effect of sintering temperatures on the same are studied. Figures 5(a), 5(b), 5(c), 5(d) show microstructural homogeneities and remarkably different morphology for SnO_2 powder with different sintering temperatures. To avoid the confusion and get the clear idea of the crystal growth, only few SEM images are given, namely, of samples a, b, c, and d. It is clearly seen that the crystal size of the nanoparticles goes on increasing as the sintering temperature increases. At the initial stages seen in samples a and b, the crystalline size is of only few nanometers, whereas at higher temperatures the size of nanoparticles increases to around 17 nm. The uniformity in the crystal size of the samples prepared in all the calcinated samples is observed and hence the practical production of uniformed size nanoparticles of SnO_2 can be developed, for an industrial application. The grain size of the nanoparticles varied within a few nanometer ranges and is totally depending on the sintering temperatures with linearity.

Figure 6(a) shows a low resolution TEM image whose inset is the magnified image. In Figure 6(b) the high resolution TEM image of SnO_2 is shown. One micron square area was considered for obtaining the reflection fringes. Presence of spotted-lines instead of regular points or continuous lines have proven the nanostructure of SnO_2. The calculated interplanar 0.41 and 0.39 nm spacings were close to that of interplanar spacing of (110) and (101) reflection planes (0.411 and 0.391 nm), respectively, of SnO_2. Unclear but uniform reflection circle was due to nanocrystalline form of SnO_2; as for amorphous metal oxide, fuzzy pattern is dominant whereas distinct regular spot is commonly seen in crystalline oxides. The EDAX pattern in Figure 6(d) is recorded while TEM analysis has confirmed an existence of Sn and O element in 57 and 33 wt % ratio.

Figure 7 shows room temperature photoluminescence spectrum of SnO_2 nanopowders in the range of 290–550 nm. Strong peak at 413 and weak peak at 446 and 474 nm are nearly equal to earlier report [29]. It is clear that the two strong peaks at 446 and 474 nm may be due to luminescence centers, such as the presence of nanocrystal or defects in

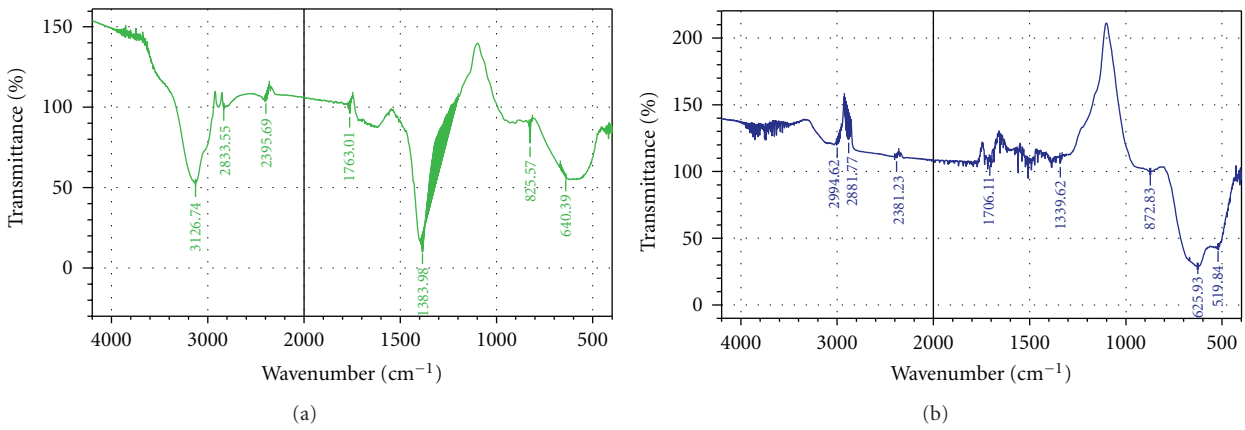

Figure 4: FT-IR spectrum of SnO_2 nanoparticle prepared by sol-gel method (a) as prepared and (b) sintered at 873 K.

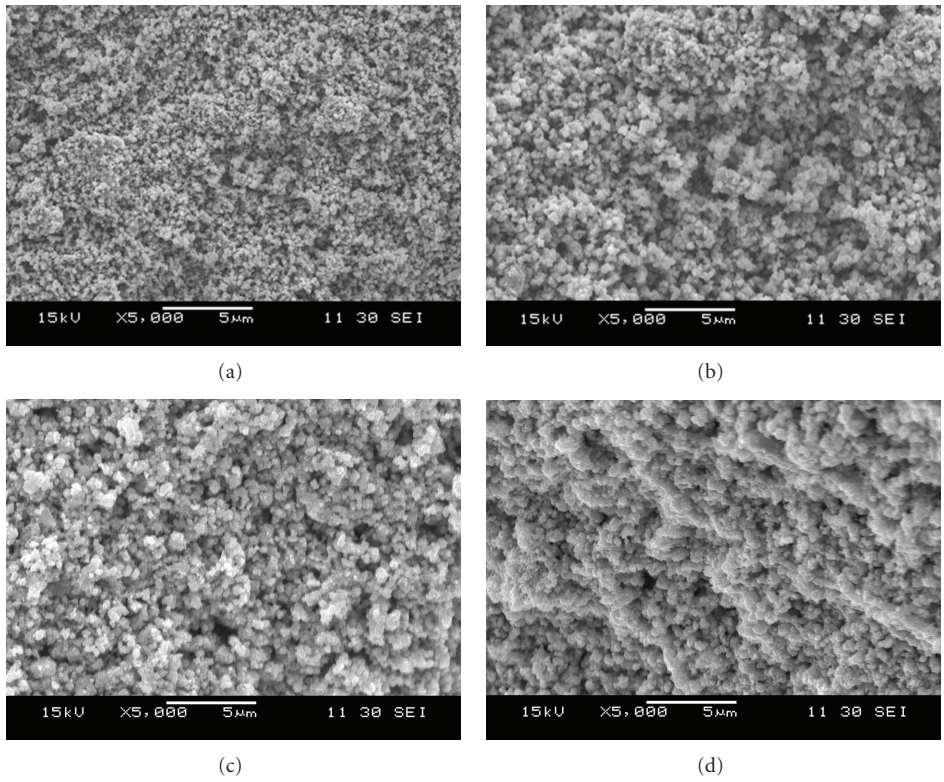

Figure 5: SEM image of SnO_2 nanoparticles synthesized by sol-gel method (a) as prepared, (b) sintered at 573 K, (c) sintered at 873 K (d), and sintered at 1073 K.

SnO_2 nanogranules and are important in application of this powder in optoelectronic devices, but that is not yet clear.

We propose the possible mechanism of formation of the SnO_2 nanoparticles as discussed below. The growth of SnO_2 from tin chloride dihydrate precursor using sol-gel process generally undergoes four stages, such as solvation, hydrolysis, polymerization, and transformation into SnO_2. The tin chloride dihydrate precursor was first solvated into HNO_3 along with citric acid dihydrate to form tin citrate complex. From (2), the addition of ammonium hydroxide neutralizes the excess acid that remains in solution. After refluxing, the tin citrate complex breaks down and tin hydroxide is formed (3). Thus formed tin hydroxide after calcination forms tin oxide with removal of water as shown in (4):

$$SnCl_2 \longrightarrow SnCl_4 \longrightarrow \text{Sn-Citrate} \quad (2)$$

$$\text{Sn-Citrate} \longrightarrow Sn(OH)_4 + H_2O \quad (3)$$

$$Sn(OH)_4 \longrightarrow SnO_2 + 2H_2O \quad (4)$$

The hydrolysis and condensation generally occur fast and need to be inhibited for avoiding precipitation and

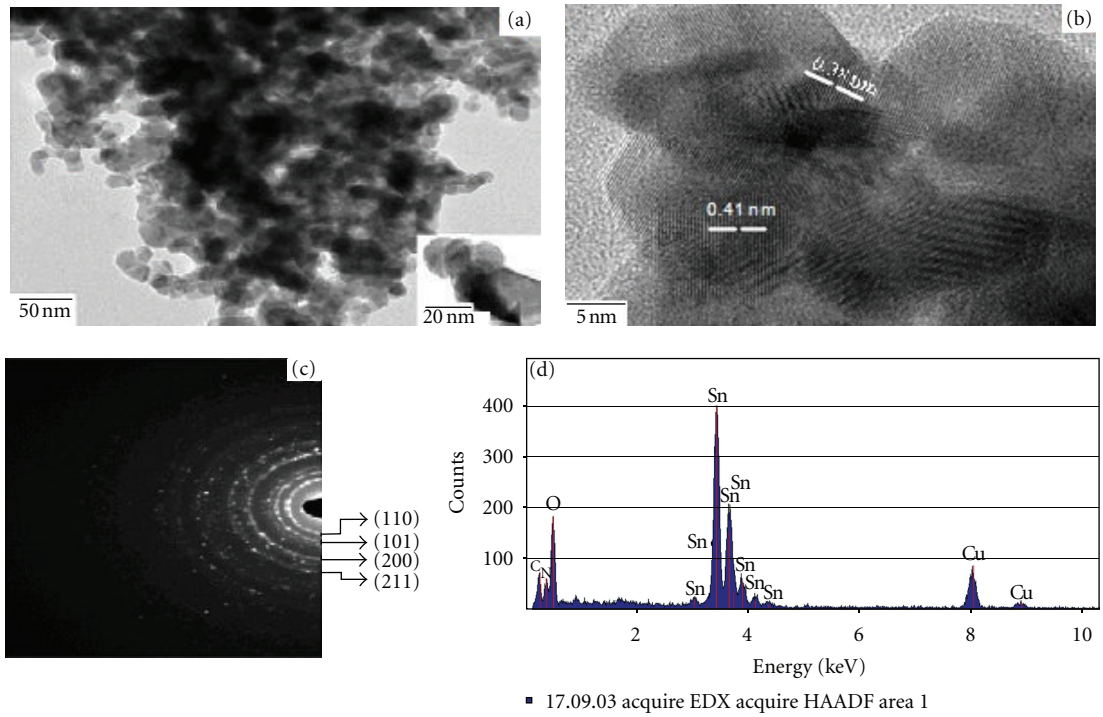

Figure 6: (a) TEM, (b) HR-TEM, (c) SAED, (d) EDAX measurements of SnO_2 nanoparticles synthesized by sol-gel method.

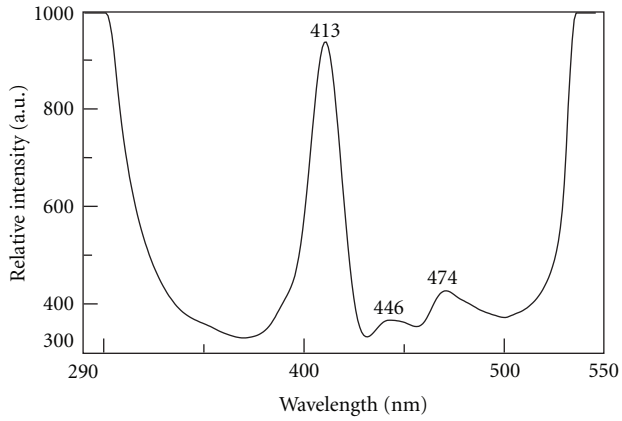

Figure 7: Room temperature photoluminescence spectrum of SnO_2 nanoparticles synthesized by sol-gel method.

allowing the sol-gel formation. The gel is based on polymeric formation with ≡Sn-Sn-O≡ bond which appears as a result of oleation of the hydroxyl complex, $Sn(OH)_n$ with subsequent polymerization with the splitting of water molecule. The increase in the number of bridge bonds, occurring in the gelation stage, is also continued under the action of temperature in the course of thermal treatment. The dehydration process can be described by the following scheme [30]:

$$2(\equiv \text{Sn-OH})_n = (\equiv \text{Sn-Sn-O} \equiv)_n + n\text{H}_2\text{O}. \quad (5)$$

The inorganic network of freshly prepared gels retains considerable amount of liquid of the liquid-phase, composed of water; hence, the gel is dried at 373 K for 5 hours. Citric acid is widely used as complexing agent. Citric acid (H_3L) is a weak triprotic acid and dissociates in a stepwise manner in a solution depending upon the pH of the solution. Only when the pH value of the solution is above 6.4, species L becomes a dominant one [31]. The complexation reactions between the metal ion and citric acid are also highly dependent upon pH and cannot occur at very strong acidic conditions. Thus, we adjusted the pH value of the solution to ~9. Another advantage of this basic condition is that the isoelectric point of the SnO_2 powder lies at a pH of 2.5–3.7 [27, 32, 33]. The strong acidic condition enhances the hydrogen bonding among the protonated nanocrystallites leading to a high degree of agglomeration among freshly prepared nanocrystallites. The chelated tin has six-fold coordination available for reacting while 4 fold is available in an inorganic starting material so its reactivity is greatly lowered [34, 35].

The general formula is M(OOR)*n* (M-refers to Sn), and when sol was refluxed at 373 K, the solution changed slowly into gel; the controlled sol-gel process can be described as follows [36]:

hydrolysis:

$$\text{M(OOR)}_n + x\text{H}_2\text{O} \longrightarrow \text{M(OOR)}_{n\text{-}x}(\text{OH})_x + x\text{RCOOH} \quad (6)$$

condensation:

$$2\text{M(OOR)}_{n\text{-}x}(\text{OH})_x \longrightarrow [(\text{OH})_{x-1}(\text{OOR})_{n\text{-}x}\text{M}]\text{O} + \text{H}_2\text{O}. \quad (7)$$

When the dried gels were heat-treated at different calcinating temperatures, nanocrystalline SnO_2 having very small size and very high surface areas was obtained. Upon heating at higher temperature, the specific surface area of the sol-gel-obtained nanocrystalline SnO_2 decreased, especially at above 773 K which can be explained as follows. In citric acid-based sol-gel method, the complexing ligand may also act as a surface protecting agent, protecting the newly transformed nanocrystalline SnO_2 from agglomeration at lower temperature, but when heated to high temperature, the citric acid is destroyed, its protecting property is lost, and the SnO_2 nanocrystals starts agglomerating resulting into an increase in its size.

4. Conclusion

Using sol-gel method nanocrystalline SnO_2 powder has been successfully synthesized. The synthesized SnO_2 nano-powder was analyzed at 373–1073 K calcining temperature. Oxide phase formation has been confirmed from FT-IR studies. Particle size was confirmed through TEM. X-ray diffraction pattern confirms the tetragonal structure of SnO_2. Thus, this synthesis method is fast, simple, convenient and is feasible on industrial scale to synthesize SnO_2 nanomaterial. The possible applications of SnO_2 nanoparticles are in gas sensor, solar cells, optoelectronic devices, paint industry, and surface coating industry.

Acknowledgments

One of the authors (B. G. Pawar) acknowledges the Department of Atomic Energy, Board of Atomic Research in Nuclear Science (Grant Sanction no. 2008/36/83/-BRNS/4009), Government of India. The authors are also grateful to University Grants Commission, New Delhi, and Department of Science and Technology, Government of India, for SAP and DST-FIST programme facilities.

References

[1] H. J. Ahn, H. C. Choi, K. W. Park, S. B. Kim, and Y. E. Sung, "Investigation of the structural and electrochemical properties of size-controlled SnO_2 nanoparticles," *Journal of Physical Chemistry B*, vol. 108, no. 28, pp. 9815–9820, 2004.

[2] J. Zhu, Z. Lu, S. T. Aruna, D. Aurbach, and A. Gedanken, "Sonochemical synthesis of SnO_2 nanoparticles and their preliminary study as li insertion electrodes," *Chemistry of Materials*, vol. 12, no. 9, pp. 2557–2566, 2000.

[3] B. Cheng, J. M. Russell, W. Shi, L. Zhang, and E. T. Samulski, "Large-scale, solution-phase growth of single-crystalline SnO_2 nanorods," *Journal of the American Chemical Society*, vol. 126, no. 19, pp. 5972–5973, 2004.

[4] A. Kay and M. Gratzel, "Dye-sensitized core-shell nanocrystals: improved efficiency of mesoporous tin oxide electrodes coated with a thin layer of an insulating oxide," *Chemistry of Materials*, vol. 14, no. 7, pp. 2930–2935, 2002.

[5] G. Micocci, A. Serra, P. Siciliano, A. Tepore, and Z. A. Adib, "CO sensing characteristics of reactively sputtered SnO_2 thin films prepared under different oxygen partial pressure values," *Vacuum*, vol. 47, no. 10, pp. 1175–1177, 1996.

[6] V. Demarne and A. Grisel, "A new temperature deposition technique for integrated sensors," *Sensors and Actuators B*, vol. 15-16, pp. 63–67, 1993.

[7] S. H. Park, Y. C. Son, W. S. Willis, S. L. Suib, and K. E. Creasy, "Tin oxide films made by physical vapor deposition-thermal oxidation and spray pyrolysis," *Chemistry of Materials*, vol. 10, no. 9, pp. 2389–2398, 1998.

[8] C. Goebbert, M. A. Aegerter, D. Burgard, R. Nass, and H. Schmidt, "Ultrafiltration conducting membranes and coatings from redispersable, nanoscaled, crystalline SnO_2: Sb particles," *Journal of Materials Chemistry*, vol. 9, no. 1, pp. 253–258, 1999.

[9] C. Terrier, J. P. Chatelon, R. Berjoan, and J. A. Roger, "Sb-doped SnO_2 transparent conducting oxide from the sol-gel dip-coating technique," *Thin Solid Films*, vol. 263, no. 1, pp. 37–41, 1995.

[10] A. Gamard, O. Babot, B. Jousseaume, M. C. Rascle, T. Toupance, and G. Campet, "Conductive F-doped tin dioxide sol—gel materials from fluorinated β-diketonate tin(IV) complexes. Characterization and thermolytic behavior," *Chemistry of Materials*, vol. 12, no. 11, pp. 3419–3426, 2000.

[11] S. S. Park and J. D. Mackenzie, "Sol-gel-derived tin oxide thin films," *Thin Solid Films*, vol. 258, no. 1-2, pp. 268–273, 1995.

[12] A. Dieguez, A. R. Rodriguez, J. R. Morante, U. Weimar, M. S. Berberich, and W. Gopel, *Sensors and Actuators B*, vol. 3, p. 11, 1996.

[13] M. I. Ivanovskaya, P. A. Bogdanov, D. R. Orlik, A. C. Gurlo, and V. V. Romanovskaya, "Structure and properties of sol-gel obtained SnO_2 and SnO_2-Pd films," *Thin Solid Films*, vol. 296, no. 1-2, pp. 41–43, 1997.

[14] S. G. Ansari, P. P. Boroojerdian, S. R. Sainkar, R. N. Karekar, R. C. Aiyer, and S. K. Kulkarni, "Grain size effects on H_2 gas sensitivity of thick film resistor using SnO_2 nanoparticles," *Thin Solid Films*, vol. 295, no. 1-2, pp. 271–276, 1997.

[15] D. P. Tunstall, S. Patou, R. S. Liu, and Y. H. Kao, "Size effects in the NMR of SnO_2 powders," *Materials Research Bulletin*, vol. 34, no. 10-11, pp. 1513–1520, 1999.

[16] K. Prasad, D. V. Pinjari, A. B. Pandit, and S. T. Mhaske, "Synthesis of titanium dioxide by ultrasound assisted sol-gel technique: effect of amplitude (power density) variation," *Ultrasonics Sonochemistry*, vol. 17, no. 4, pp. 697–703, 2010.

[17] A. Jitianu, Y. Altindag, M. Zaharescu, and M. Wark, "New SnO_2 nano-clusters obtained by sol-gel route, structural characterization and their gas sensing applications," *Journal of Sol-Gel Science and Technology*, vol. 26, no. 1–3, pp. 483–488, 2003.

[18] J. P. Chatelon, C. Terrier, and J. A. Roger, "Influence of elaboration parameters on the properties of tin oxide films obtained by the sol-gel process," *Journal of Sol-Gel Science and Technology*, vol. 10, no. 1, pp. 55–65, 1997.

[19] K. Prasad, D. V. Pinjari, A. B. Pandit, and S. T. Mhaske, "Phase transformation of nanostructured titanium dioxide from anatase-to-rutile via combined ultrasound assisted sol-gel technique," *Ultrasonics Sonochemistry*, vol. 17, no. 2, pp. 409–415, 2010.

[20] S. Rani, P. Suri, P. K. Shishodia, and R. M. Mehra, "Synthesis of nanocrystalline ZnO powder via sol-gel route for dye-sensitized solar cells," *Solar Energy Materials and Solar Cells*, vol. 92, no. 12, pp. 1639–1645, 2008.

[21] L. Dong, Y. C. Liu, Y. H. Tong et al., "Preparation of ZnO colloids by aggregation of the nanocrystal subunits," *Journal of Colloid and Interface Science*, vol. 283, no. 2, pp. 380–384, 2005.

[22] F. Grasset, R. Marchand, A. M. Marie, D. Fauchadour, and F. Fajardie, "Synthesis of CeO_2@SiO_2 core-shell nanoparticles

by water-in-oil microemulsion. Preparation of functional thin film," *Journal of Colloid and Interface Science*, vol. 299, no. 2, pp. 726–732, 2006.

[23] H. Shiomi, C. Kakimoto, A. Nakahira, and S. Takeda, "Preparation of SnO_2 monolithic gel by sol-gel method," *Journal of Sol-Gel Science and Technology*, vol. 19, no. 1–3, pp. 759–763, 2000.

[24] S. Chandramouleeswaran, S. T. Mhaske, A. A. Kathe, P. V. Varadarajan, V. Prasad, and N. Vigneshwaran, "Functional behaviour of polypropylene/ZnO-soluble starch nanocomposites," *Nanotechnology*, vol. 18, no. 38, Article ID 385702, 2007.

[25] D. V. Pinjari and A. B. Pandit, "Cavitation milling of natural cellulose to nanofibrils," *Ultrasonics Sonochemistry*, vol. 17, no. 5, pp. 845–852, 2010.

[26] K. J. Jarag, D. V. Pinjari, A. B. Pandit, and G. S. Shankarling, "Synthesis of chalcone (3-(4-fluorophenyl)-1-(4-methoxyphenyl)prop-2-en-1-one): advantage of sonochemical method over conventional method," *Ultrasonics Sonochemistry*, vol. 18, no. 2, pp. 617–623, 2011.

[27] J. Zhang and L. Gao, "Synthesis and characterization of nanocrystalline tin oxide by sol-gel method," *Journal of Solid State Chemistry*, vol. 177, no. 4-5, pp. 1425–1430, 2004.

[28] K. C. Song and Y. Kang, "Preparation of high surface area tin oxide powders by a homogeneous precipitation method," *Materials Letters*, vol. 42, no. 5, pp. 283–289, 2000.

[29] J. Q. Hu, X. L. Ma, N. G. Shang et al., "Large-scale rapid oxidation synthesis of SnO_2 nanoribbons," *Journal of Physical Chemistry B*, vol. 106, no. 15, pp. 3823–3826, 2002.

[30] L. F. Chepik, E. P. Troshina, T. S. Mashchenko, D. P. Romanov, A. I. Maksimov, and O. F. Lutskaya, "Crystallization of SnO_2 produced by sol-gel technique from salts of tin in different oxidation states," *Russian Journal of Applied Chemistry*, vol. 74, no. 10, pp. 1617–1620, 2001.

[31] J. H. Choy and Y. S. Han, "Citrate route to the piezoelectric $Pb(Zr,Ti)O_3$oxide," *Journal of Materials Chemistry*, vol. 7, no. 9, pp. 1815–1820, 1997.

[32] C. Gobbert, M. A. Aegerter, D. Burgard, R. Nass, and H. Schmid, "Ultrafiltration conducting membranes and coatings from redispersable, nanoscaled, crystalline SnO_2:Sb particles," *Journal of Materials Chemistry*, vol. 9, no. 1, pp. 253–258, 1999.

[33] M. J. Bommmel, W. A. Groen, H. A. Vanhal, W. C. Keur, and T. M. Bernards, "The electrical and optical properties of thin layers of nano-sized antimony doped tinoxide particles," *Journal of Materials Science*, vol. 34, no. 19, pp. 4803–4809, 1999.

[34] S. De Monredon, A. Cellot, F. Ribot et al., "Synthesis and characterization of crystalline tin oxide nanoparticles," *Journal of Materials Chemistry*, vol. 12, no. 8, pp. 2396–2400, 2002.

[35] L. Broussous, C. V. Santilli, S. H. Pulcinelli, and A. F. Craievich, "SAXS study of formation and growth of tin oxide nanoparticles in the presence of complexing ligands," *Journal of Physical Chemistry B*, vol. 106, no. 11, pp. 2855–2860, 2002.

[36] W. X. Kuang, Y. N. Fan, K. W. Yao, and Y. Chen, "Preparation and characterization of ultrafine rare earth molybdenum complex oxide particles," *Journal of Solid State Chemistry*, vol. 140, no. 2, pp. 354–360, 1998.